Simulation of a Polymer-Free DRIE Process Using SF_6/O_2 Plasma Etching

Tobias Reiter[1]*, Alexander Toifl[2], Andreas Hössinger[2], and Lado Filipovic[1]
[1]CDL for Multi-Scale Process Modeling of Semiconductor Devices and Sensors at the Institute for Microelectronics, TU Wien, 1040 Vienna, Austria
[2]Silvaco Europe Ltd., Silvaco Inc., St Ives, Cambridgeshire, PE27 5JL, United Kingdom
*Email: reiter@iue.tuwien.ac.at

***Abstract*—We present a feature-scale simulation of the cyclic polymer-free deep-reactive ion etching (DRIE) process titled CORE which was experimentally demonstrated in [1]. The CORE process consists of four steps: Clear, Oxidize, Remove, Etch, and is based on the Bosch etching principle, whereby polymer deposition is replaced with minimal surface oxidation. Our simulation approach combines a Langmuir-type SF_6/O_2 etching model with Monte Carlo ray tracing for ballistic flux calculation and is implemented in the level-set-based topography simulator ViennaPS. Essential for the CORE process is the surface oxidation step, which we model by tracking an oxide thickness surface property in the context of the Langmuir-type surface model. We demonstrate the model's capabilities by reproducing experimental etch profiles over multiple CORE cycles.**

***Index Terms*—Topography Simulation, Plasma Etching, Bosch Process, MEMS**

I. Introduction

High-aspect-ratio (HAR) plasma etching is critical in microfabrication, especially in the production of micro-electro-mechanical systems (MEMS), sensors, and advanced logic or memory devices. Silicon deep reactive ion etching (DRIE) processes are commonly used to define narrow and high-depth features with vertical sidewalls [2], [3]. Traditionally, the Bosch process, a DRIE technique based on alternating cycles of etching (e.g., SF_6 plasma) and polymer deposition (e.g., C_4F_8 plasma), has been employed to achieve these goals due to its excellent anisotropy and throughput [4], [6].

Despite its industrial success, the Bosch process suffers from several well-known drawbacks. These include the formation of fluorocarbon residues at the feature openings, sidewall roughness due to scalloping, and the need for polymer removal post-process. Moreover, process drift can occur due to polymer accumulation on the chamber walls, leading to inconsistent results over time [1], [4].

To address these issues, Nguyen et al. proposed the CORE process in [1], a fluorocarbon-free deep silicon etching method based on cyclic switching between SF_6 and O_2 plasmas. The process consists of four steps: Clear, Oxidize, Remove, and Etch. In contrast to the Bosch process, CORE replaces the polymer deposition step with a self-limiting surface oxidation step using oxygen plasma. This modification enables operation at room temperature, which simplifies tool requirements and avoids complications associated with alternate ways of increasing sidewall protection, such as cryogenic systems. The absence of fluorocarbon deposition prevents residual particulate accumulation and helps maintain a clean reactor environment, minimizing process drift over time. Furthermore, this approach addresses significant environmental concerns by eliminating the use of fluorocarbon gases, which are often potent greenhouse gases with a high Global Warming Potential (GWP) [5]. The oxidized surface provides passivation similar to polymer inhibitors but with better stability and fewer contamination concerns.

Due to the complex combination of chemical and physical effects involved in the CORE process, accurate simulation requires more than simple empirical or geometric models. In this work, we present a topography simulation of the CORE process using the level-set based framework ViennaPS [9]. The simulator incorporates a Monte Carlo ray tracing method to compute particle fluxes and applies a Langmuir-type surface reaction model to determine local etch rates. Oxidation is modeled as a spatially varying scalar surface property, allowing efficient tracking of oxide growth and removal during the process cycle.

We demonstrate the ability of the model to reproduce experimentally measured profiles and explore the influence of etch parameters on the resulting topography. The simulation framework provides insight into the physical mechanisms of the process and offers a useful tool for optimizing polymer-free directional silicon etching.

II. Methods

The model assumes ballistic transport of particles and Langmuir-type surface adsorption [8]. Particle transport, calculated by top-down Monte Carlo ray tracing, is separated into two main components: neutral radicals and ions. Neutral species (e.g. fluorine and oxygen radicals) diffuse through the chamber and reach the surface with a cosine angular distribution. Ions are accelerated through the sheath and thus follow a directional power-cosine distribution [5]. Their initial energy is drawn from a Gaussian distribution around a mean initial ion energy E_i. While neutral radicals reflect diffusely from the surface, ions follow a coned specular reflection, as described in [7]. The functional dependence of the re-emitted energy distribution on the incident energy is also described in detail in [7].

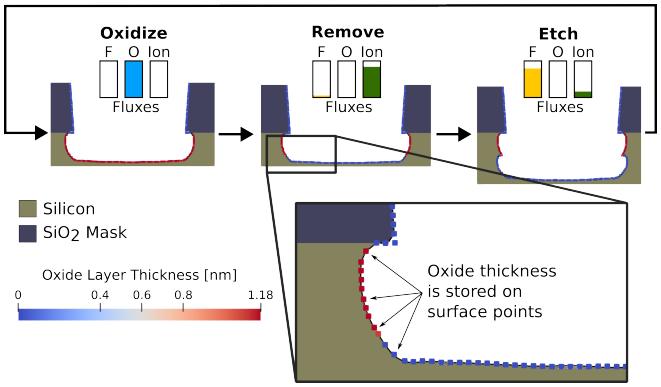

Fig. 1. Visualization of the simulated **Oxidize**, **Remove**, and **Etch** steps during one CORE cycle on a trench geometry. The oxide thickness is treated as a surface property and is visualized as a color map representing oxide thickness. During the remove step, the oxide is stripped, and the subsequent etch step removes Si based on the local surface state. The simulation tracks the evolution of oxidation over the surface throughout the cycle.

To compute local surface reaction rates, we calculate steady-state surface coverages (e.g., $d\theta/dt = 0$) of fluorine (θ_F) and oxygen (θ_O) at each discretized time step. These coverages are given by [8]:

$$\sigma_{Si}\frac{d\theta_F}{dt} = \gamma_F\Gamma_F\left(1-\theta_F-\theta_O\right) - k\sigma_{Si}\theta_F - 2Y_{ie}\Gamma_i\theta_F \quad (1)$$

$$\sigma_{Si}\frac{d\theta_O}{dt} = \gamma_O\Gamma_O\left(1-\theta_F-\theta_O\right) - \beta\sigma_{Si}\theta_O - Y_O\Gamma_i\theta_O \quad (2)$$

Here, Γ_F, Γ_O, and Γ_i are the local fluxes of fluorine, oxygen, and positively-charged ions, respectively. k is the chemical etch rate constant, β is the oxygen recombination rate, σ_{Si} is the surface site density, Y_O and Y_{ie} are the etch yields for oxygen and ion-enhanced processes, and γ_F, γ_O are the sticking coefficients.

The local etch rate is composed of three distinct contributions:

$$\mathrm{ER} = \frac{1}{\rho_{Si}}\left(\underbrace{\frac{k\sigma_{Si}\theta_F}{4}}_{\text{Chemical}} + \underbrace{Y_p\Gamma_i}_{\text{Sputter}} + \underbrace{Y_{ie}\Gamma_i\theta_F}_{\text{Ion-enhanced}}\right) \quad (3)$$

Here, ρ_{Si} is the silicon density. The first term describes chemical etching by fluorine radicals, the second term accounts for physical sputtering by ions, and the third captures ion-enhanced etching effects, where ion bombardment activates or accelerates chemical reactions by breaking surface bonds or creating reactive sites.

We employ the level-set method [10] to track surface evolution. The interface is represented implicitly by a signed distance function $\phi(\vec{x})$, where the surface $\mathcal{S}$ corresponds to the zero level set:

$$\mathcal{S} = \{\vec{x} : \phi(\vec{x}) = 0\} \quad (4)$$

The etch rate defines the velocity field $v(\vec{x})$ used in the level-set evolution equation:

$$\frac{\partial\phi(\vec{x},t)}{\partial t} + v(\vec{x})|\nabla\phi(\vec{x},t)| = 0 \quad (5)$$

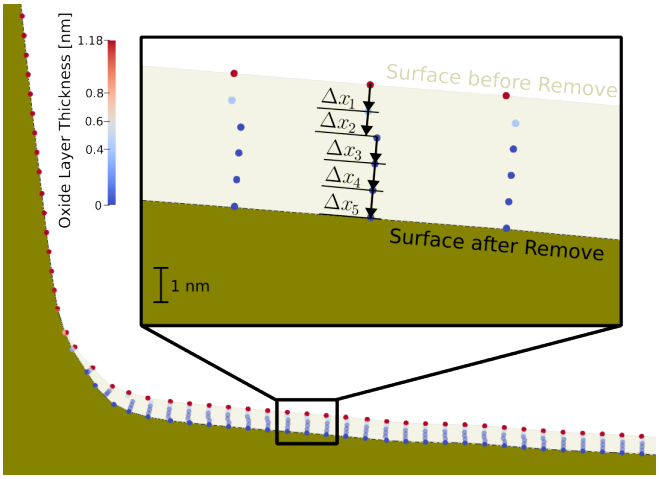

Fig. 2. Surface evolution during the Remove step. The inset illustrates the local surface displacements Δx_i used in the level-set propagation. Due to the directional ion flux, etching occurs predominantly at the bottom of the structure, while sidewalls remain largely unaffected, preserving their oxide thickness. Where etching occurs, the local oxide thickness is reduced proportionally to the surface displacement Δx_i.

The velocity field, which incorporates the etch rate given in Eq. (3), indicates the normal velocity at each surface point. To solve Eq. (5), we discretize $\phi(\vec{x})$ on a uniform grid and apply a finite-difference scheme.

In the CORE process, the physical SF_6/O_2 etching model is used during the etch, remove, and oxidize steps (c.f. Figure 1). Both the etch and remove steps involve pure SF_6 plasma to strip the passivating oxide layer. The remove step differs by using a higher ion flux and increased bias power, reflecting different reactor conditions.

Oxidation is captured by a surface property that represents the local oxide thickness. If a point is oxidized, the chemical etch component is suppressed and only sputtering and ion-enhanced etching can contribute to material removal.

III. Surface Oxidation

During the oxidize step, the surface is exposed to a low-energy O_2 plasma by applying only oxygen flux while suppressing fluorine and ion fluxes. The oxide formation rate is governed by the local oxygen surface coverage θ_O.

The uniformity of θ_O is determined by the oxygen sticking coefficient and the recombination rate, which control the adsorption kinetics and surface saturation.

To model the oxide thickness $d(t)$, we employ a modified Cabrera–Mott relation [11] fitted to ellipsometry data from [1]:

$$d(t) = \theta_O\left[d_0 + d_0'\tau\ln\left(1+\frac{t}{\tau}\right)\right], \quad (6)$$

where d_0, d_0', and τ are empirical parameters and t is the oxidation duration.

In the CORE process, surface oxidation protects feature sidewalls and improves etch selectivity. The oxide layer passivates the surface by suppressing the chemical etch component,

allowing only ion-enhanced and sputtering mechanisms to contribute to material removal. Because the oxide layer remains only a few nanometers thick, a dimension significantly smaller than the overall feature sizes, resolving it as a separate material domain adds substantial computational cost for a negligible gain in physical accuracy. Instead, the oxide is represented as a scalar surface property, with the thickness at each point given by $d(t = t_O)$, where t_O is the duration of the Oxidize step. The local thickness is proportional to the oxygen coverage: fully covered sites ($\theta_O \approx 1$) yield a complete oxide layer, while partial coverage ($0 < \theta_O < 1$) results in proportionally thinner oxide.

Each simulation step begins by computing the etch rate from local fluxes. Since these fluxes depend on the steady-state surface coverages of fluorine and oxygen, multiple flux evaluations are performed iteratively until convergence is reached. Once the coverages are determined, the surface is propagated using the level-set method by solving Eq. (5) with the etch rate from Eq. (3) as the velocity field. During propagation, the local oxide thickness is reduced according to the corresponding surface displacement Δx (c.f. Fig. 2), ensuring consistent removal of oxidized material during etching.

This method allows us to maintain a spatially-resolved oxide thickness without the overhead of tracking an additional very thin geometry layer.

IV. Results

To align the simulation with experimental data, a set of model parameters, listed in Table I, is calibrated. These include the fluorine and ion fluxes during the etch and remove steps, the mean initial ion energy, and the fluorine sticking coefficient. These parameters strongly influence the local etch rates and the resulting topography evolution. Calibration is performed by minimizing the deviation between simulated and experimentally measured profiles, as shown in Figure 3.

We then apply the calibrated model to a silicon trench etching application to evaluate its ability to reproduce experimentally observed features. Specifically, we simulate five complete CORE cycles on a single trench structure. To investigate the influence of etch duration on the resulting topography, we perform a series of four simulations with etch step durations of 2, 4, 6, and 8 minutes, respectively, while keeping the durations of the oxidize and remove steps fixed. The initial trench mask is approximated from available SEM images, assuming a width of approximately 590 nm, a height of 1.2 μm, and a slight sidewall taper of 4°.

Figure 4 shows the simulated trench profiles alongside corresponding SEM images from [1]. As expected, longer etch durations lead to deeper features and increasingly pronounced sidewall scalloping due to the cumulative effect of repeated etch cycles. The simulated profiles reproduce this trend and exhibit the characteristic scallop pattern observed in experiments, indicating that the model can accurately reflect the interplay between ion-enhanced etching, surface oxidation, and sputtering.

We also analyze intermediate profiles after each individual CORE cycle. As shown in the intermediate profile lines of Figure 4, the trench depth increases almost linearly with each cycle, while the scalloping becomes more defined and periodic.

To demonstrate the three-dimensional capability of the model, we apply the same CORE sequence to a pillar array geometry consisting of multiple cylindrical features arranged in a regular grid. The simulation results, shown in Figure 5, exhibit characteristic features such as slight tapering, anisotropic etching, and uniform profile evolution across the array. These features are consistent with experimental observations reported in [1], highlighting the model's ability to accurately reproduce complex 3D topographies.

The three-dimensional simulation of the pillar array was performed on a domain with a total extent of 1 μm in both lateral directions. Each pillar was defined by a cylindrical mask with a diameter of 0.9 μm. The level-set grid used a uniform spacing of 10 nm, resulting in a high-resolution representation of the evolving surface. With this setup, the simulation of five complete CORE cycles required approximately 8 minutes and 40 seconds on a workstation equipped with a 12th Gen Intel® Core™ i7-12700K CPU (8 P-cores + 4 E-cores, 20 threads).

TABLE I
PARAMETERS USED IN THE MODEL. PARAMETERS WITHOUT REFERENCE WERE FITTED TO MATCH THE EXPERIMENTAL RESULTS FROM [1]

Parameter	Description	Value
Γ_F^{E}	Fluorine flux during Etch	15.4×10^{15} cm^{-2} s^{-1}
Γ_i^{E}	Ion flux during Etch	1.1×10^{15} cm^{-2} s^{-1}
Γ_i^{R}	Ion flux during Remove	15×10^{15} cm^{-2} s^{-1}
γ_F	Fluorine sticking coefficient	0.8
E_{i}	Mean initial ion energy	30 eV
$k\sigma_{Si}$	Chemical etch rate constant	3×10^{17} cm^{-2} s^{-1} [8]
γ_O	Oxygen sticking coefficient	1 [8]
$\beta\sigma_{Si}$	Oxygen recombination constant	4×10^{13} cm^{-2} s^{-1} [8]
d_0	Initial oxide thickness	1.1 nm [1]
d_0'	Initial oxide growth rate	0.03 nm s^{-1} [1]
τ	Oxidation time constant	10 s [1]

V. Conclusion

We presented a feature-scale simulation framework for the polymer-free CORE plasma etching process using SF_6/O_2 chemistry. By combining a Langmuir-type surface reaction model with Monte Carlo ray tracing and level-set topography evolution, our approach captures the cyclic nature of the Oxidize, Remove, and Etch steps. A key contribution is the efficient modeling of surface oxidation as a spatially-resolved scalar property, enabling selective etching behavior without the

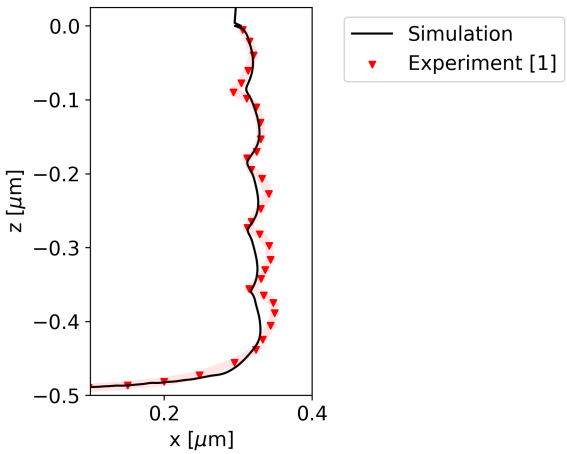

Fig. 3. Comparison of simulated and experimental profiles with an etch time of 6 minutes each cycle. The image shows one sidewall at the bottom of the etched trench.

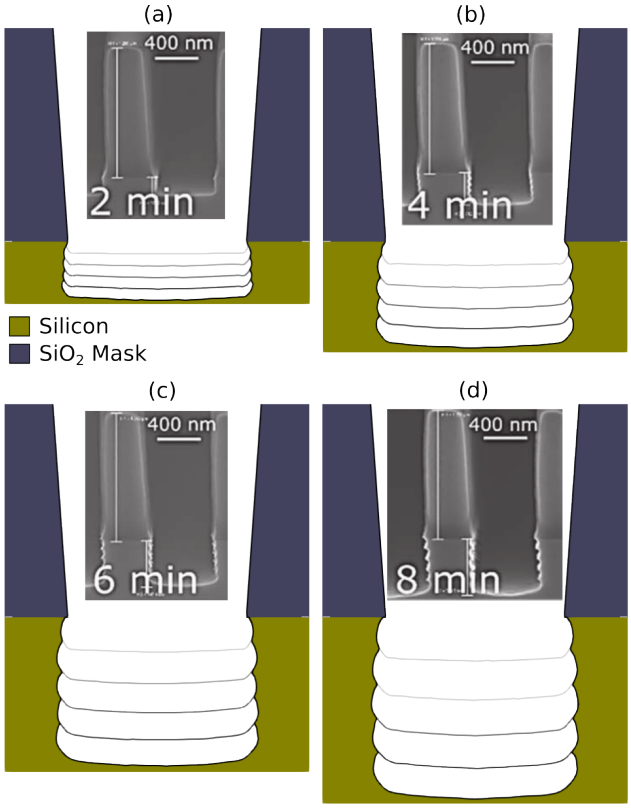

Fig. 4. Simulated trench profiles after five CORE cycles for etch step durations of 2, 4, 6, and 8 minutes. Longer etch times result in deeper trenches and more pronounced scalloping. The profile evolution qualitatively matches experimentally observed structures from [1]. © The Electrochemical Society. Reproduced by permission of IOP Publishing Ltd. All rights reserved.

need for an explicit oxide geometry layer. Calibration against experimental data confirms that the model reproduces critical topographic features, such as sidewall scalloping and depth

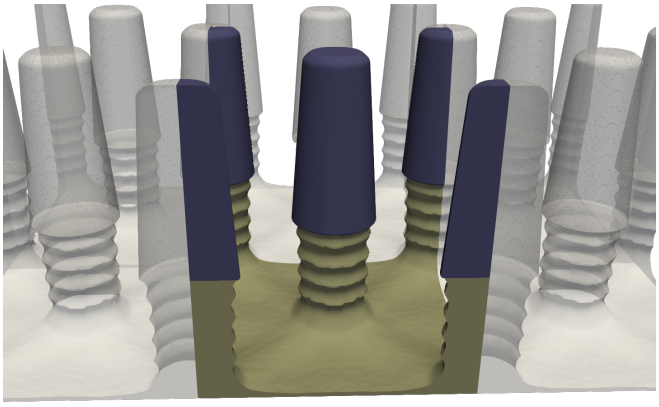

Fig. 5. Simulated etch result on a pillar array, similar to the result presented in [1], after five CORE cycles, demonstrating the 3D capabilities of the model.

evolution over multiple cycles. These results demonstrate the potential of the presented model to support predictive process design and optimization in advanced silicon etching applications.

Acknowledgment

Financial support by the Federal Ministry of Labour and Economy, the National Foundation for Research, Technology and Development, and the Christian Doppler Research Association is gratefully acknowledged.

References

[1] V. T. H. Nguyen, C. Silvestre, P. Shi, R. Cork, F. Jensen, J. Hubner, K. Ma, P. Leussink, M. de Boer, and H. Jansen, "The CORE Sequence: A Nanoscale Fluorocarbon-Free Silicon Plasma Etch Process Based on SF_6/O_2 Cycles with Excellent 3D Profile Control at Room Temperature," ECS J. Solid State Sci. Technol. 9, 2020.

[2] B. Wu, A. Kumar, and S. Pamarthy, "High aspect ratio silicon etch: A review," J. Appl. Phys. 108, 2010.

[3] S. Gomez, R. J. Belen, M. Kiehlbauch, and E. S. Aydil, "Etching of high aspect ratio structures in Si using SF_6/O_2 plasma ," J. Vac. Sci. Technol. A 22, 2004.

[4] H. V. Jansen, M. de Boer, S. Unnikrishnana, M. C. Louwerse, and M. C. Elwenspoek, "Black silicon method X: a review on high speed and selective plasma etching of silicon with profile control: an in-depth comparison between Bosch and cryostat DRIE processes as a roadmap to next generation equipment," J. Micromech. Microeng. 19, 2009.

[5] V. M. Donnelly, and A. Kornblit, "Plasma etching: Yesterday, today, and tomorrow," J. Vac. Sci. Technol. A 31, 2013.

[6] B. Chang, F. Jensen, J. Hübner, and H. Jansen, "DREM2: a facile fabrication strategy for freestanding three dimensional silicon micro- and nanostructures by a modified Bosch etch process," J. Micromech. Microeng. 28, 2018.

[7] R. J. Belen, S. Gomez, M. Kiehlbauch, D. Cooperberg, and E. S. Aydil, "Feature-scale model of Si etching in SF_6 plasma and comparison with experiments" J. Vac. Sci. Technol. A: Vac. Surf. Films 23, 2005.

[8] R. J. Belen, S. Gomez, D. Cooperberg, M. Kiehlbauch, and E. S. Aydil, "Feature-scale model of Si etching in SF_6/O_2 plasma and comparison with experiments," J. Vac. Sci. Technol. A: Vac. Surf. Films 23, 2005.

[9] T. Reiter *et al.*, ViennaPS 3.4.0 2025

[10] J. A. Sethian, "Level Set Methods and Fast Marching Methods: Evolving Interfaces in Computational Geometry, Fluid Mechanics, Computer Vision, and Materials Science", 2nd Edition, Cambridge University Press, Cambridge, U.K., 1999.

[11] F. P. Fehlner, and N. F. Mott, "Low-temperature oxidation," Oxid. Met. 2, 1970.